ELSEVIER

Surface and Coatings Technology 124 (2000) 210–221

SURFACE & COATINGS TECHNOLOGY

www.elsevier.nl/locate/surfcoat

Enhancement of mechanical properties of TiN/AlN multilayers by modifying the number and the quality of interfaces

Anne Thobor [a,*], Christophe Rousselot [a], Christine Clement [a], Jamal Takadoum [b], Nicolas Martin [c], Rosendo Sanjines [c], Francis Levy [c]

[a] *Laboratoire de Métrologie des Interfaces Techniques (LMIT), Institut des Traitements de Surface de Franche-Comté (ITSFC), 4 place Lucien Tharradin, F-25200 Montbeliard, France*

[b] *Laboratoire de Microanalyse des Surfaces (LMS), Institut des Traitements de Surface de Franche-Comté (ITSFC), ENSMM, 26 rue de l'épitaphe, F-25030 Besancon, France*

[c] *Institut de Physique Appliquée (IPA), Ecole Polytechnique Fédérale de Lausanne (EPFL), CH-1015 Lausanne, Switzerland*

Received 19 July 1999; accepted 24 November 1999

Abstract

The influence of a post layer-deposition ion bombardment (PLDIB) etching process on the morphology and mechanical properties of TiN/AlN multilayers has been studied. TiN/AlN multilayers have been deposited by reactive direct-current (DC) magnetron sputtering with and without the PLDIB etching process and characterised by scanning electron microscopy (SEM), atomic force microscopy (AFM) and glow discharge optical emission spectroscopy (GDOES). Scratch tests, hardness and wear resistance measurements of the coatings have also been performed. The relevant parameters appear to be the degree of roughness of the interfaces and the thickness of the TiN+AlN total period. Smooth interlayer surfaces and thin period thickness (120 nm) significantly improve the mechanical properties (hardness, wear resistance and critical load) of the TiN/AlN multilayers. These results demonstrate that a combination of DC sputtering with the PLDIB etching process constitutes an effective method for optimising the mechanical properties of TiN/AlN multilayers.

Keywords: Ion bombardment; Interfacial roughness; Mechanical properties; Reactive sputtering; TiN/AlN multilayers

1. Introduction

Over the past few years there has been growing interest in the synthesis of hard coatings materials such as transition metal nitrides, carbides, oxides or borides. The main uses of these materials cover the field of wear as well as friction reduction, and are closely linked to the combination of hardness and low friction coefficient. In particular, hard coatings such as TiN have been used in the protection of tools for machining, cutting, forging and forming technologies. It is also an attractive material to reduce adhesive wear. However, TiN films tend to oxidise at temperatures above 500°C and, consequently, the protective ability of the coating is strongly reduced [1–3]. Addition of aluminium to TiN improves its oxidation resistance and increases the temperature range of possible applications [1,4–6]. In fact, TiAlN coatings used at high temperatures exhibit a dense, highly adhesive and protective Al_2O_3 film on the surface due to diffusion of oxygen in the bulk [7–9]. However, TiAlN coatings show poor performance in the case of low sliding speed or interrupted cutting processes as a consequence of their brittleness and high friction coefficient.

Multilayered thin films belong to the promising surface technologies developed to optimise and/or enhance coatings for high requirements [10–12]. Jensen et al. [13] showed that a TiN/AlN multilayered structure greatly improves the significance performance of single-layered TiAlN [10]. Several reasons argue for advantages of multilayered films [13–17]. First, interface layers can be used to improve the adhesion of a coating to the substrate. The deposition of several thin layers with different mechanical properties allows the designer to meet complex requirements such as hardness, toughness, wear resistance or adhesion. Last but not least, interfacial areas favour stress relaxation and prevent the propagation of cracks.

The aim of present paper is to show the role of the

* Corresponding author. Tel.: +33-3-81-994696; fax: +33-3-81-994673.
E-mail address: anne.thobor@pu-pm.univ-fcomte.fr (A. Thobor)

0257-8972/00/$ - see front matter
PII: S0257-8972(99)00655-6

period thickness ($\Lambda = \lambda_{TiN} + \lambda_{AlN}$) and the influence of interface structure, roughness and composition on some mechanical properties of TiN/AlN multilayered coatings. Two series of multilayers have been produced with equal TiN and AlN sub-layer thicknesses ($\lambda_{TiN} = \lambda_{AlN}$). The first one (type I) concerns simple alternations of each metallic nitride prepared by direct-current (DC) reactive sputtering and for various period thicknesses (Λ). For the second (type II), ion bombardment of the film has been applied between the deposition of each TiN and AlN sub-layer. The effect of the total period on tribological and mechanical properties of the coatings is well established, and benefits of ion bombardment are also proved. Finally, the quality and features of the sub-layer interfaces are discussed.

Table 1
Deposition parameters

Target-to-substrate distance (m)	0.06
Ti and Al target diameter (m)	0.2
Working pressure (Pa)	0.7
Nitrogen flow rate (sccm)	4
Argon flow rate (sccm)	30
DC current density on Ti target ($A\ m^{-2}$)	35
DC current density on Al target ($A\ m^{-2}$)	51
TiN (type I) deposition rate ($Å\ s^{-1}$)	2.1
AlN (type I) deposition rate ($Å\ s^{-1}$)	5.3
TiN (type II) deposition rate ($Å\ s^{-1}$)	1.7
AlN (type II) deposition rate ($Å\ s^{-1}$)	4.3
Radio-frequency (RF) bias voltage after deposition of each sub-layer (V)	−150
Argon-ion current density on TiN film ($A\ m^{-2}$)	7.4
Argon-ion current density on AlN film ($A\ m^{-2}$)	4.2

2. Experimental details

2.1. Multilayer coatings deposition

Multilayered coatings have been prepared with an SCM 650 magnetron sputtering system (Alcatel) consisting of a stainless-steel vacuum chamber ($100\ dm^3$). Argon and nitrogen were used as sputtering and reactive gas, respectively, and titanium (99.6%) and aluminium (99.5%) targets were powered by a DC generator with a constant power of 400 W. Prior to deposition, the chamber was pumped down to 10^{-5} Pa. Argon was introduced in order to get a constant argon partial pressure of 0.6 Pa and a discharge ignited to presputter the target. Then, nitrogen was injected to get a total sputtering pressure of 0.7 Pa and to fully poison the surface of the target. Argon and nitrogen mass flow rates were controlled with a mass flowmeter (MKS) and pressures measured with Pirani, Penning and Baratron pressure gauges. The optimum target–substrate distance (highest deposition rate) has been kept at 60 mm. TiN/AlN films were deposited on various substrates: (100) silicon wafer, glass and X85WMoCrV6542 high-speed steel. The latter has a hardness of 800 Hv. It was first polished with SiC paper. Smooth surfaces with a roughness of $R_a = 0.03$ μm were obtained after polishing the steel substrates with diamond pastes down to 1 μm. Each substrate was cleaned with acetone and alcohol. The deposition parameters used for the production of TiN/AlN multilayers of type I and type II are given in Table 1. For the multilayers of type II, the argon-ion current density on the TiN or AlN film was calculated according to the procedure described in previous papers [18,19]. The total thickness of the deposited films was measured mechanically with a Dektak 3030 profilometer. The deposition rate has been calculated from the thickness and the sputtering time.

Various methods are used to deposit multilayers. The most common way consists in implementing a rotating substrate holder facing each target alternately [10,20–25]. Other authors modulate the sputtered fluxes impinging on a fixed substrate with a controlled shutter moving above the targets [26]. In this study, TiN/AlN multilayers were prepared by positioning the substrate in a static mode in front of each target. The thickness of a single layer was varied by changing the deposition time and keeping the deposition rate constant. Samples of type I were prepared without any treatment between the deposition of TiN and AlN layers, whereas the type II samples involved an argon-ion bombardment of the deposited layer by polarising (RF) the substrate holder at −150 V ($E_{Ar+} = 160$ eV) for the same time as the deposition step and by stopping the target discharge. For both sample types, the period thickness Λ was varied and the ratio $\lambda_{TiN}/\lambda_{AlN}$ (TiN thickness/AlN thickness) was fixed at unity in all cases. The total multilayered thickness was kept constant in a range of 2–2.8 μm. The first layer is TiN and the last one AlN (see Table 2).

2.2. Mechanical measurements

The mechanical properties of the TiN/AlN coatings have been tested by wear tests, scratch tests and nanoindentation. Hardness values were obtained from Vickers nanohardness measurements (Nano-Tester-NHT-CSEM). The applied load was 60 mN and the loading rate was $120\ mN\ min^{-1}$. Hardness analyses also enabled us to determine Young's modulus E for an assumed Poisson's coefficient v ($v = 0.3$ in our case).

The tribometer used in this study is a ball-on-disc model. The sample was rotated in an alternative motion on a quarter circle. For the wear test procedure, a 5 mm diameter 100C6 steel bearing ball was used as counterpart. A special test equipment provides the opportunity to monitor the coefficient of friction continuously. Moreover, as the motion is alternative, the force sensor is activated in traction and in compression. Each test

Table 2
Number of TiN/AlN bilayers and estimated thickness (from deposition rate) of the period $\Lambda = \lambda_{TiN} + \lambda_{AlN}$ for the two series of multilayers. For the multilayer of type II, the deposition time and the bombardment time of each layer have the same value

Type I			Type II		
Period, Λ ($\pm$10 nm)	Number of bilayers TiN/AlN	Deposition time per bilayer TiN + AlN (min)	Period, Λ ($\pm$10 nm)	Number of bilayers TiN/AlN	Deposition time + bombardment time per bilayer TiN + AlN (min)
190	14	8 + 3.2	110	16	(8 + 8) + (3.2 + 3.2)
360	7	16 + 6.3	240	6	(16 + 16) + (6.3 + 6.3)
510	5	22.4 + 8.8	420	6	(22.4 + 22.4) + (8.8 + 8.8)
700	4	28 + 11	510	5	(28 + 28) + (11 + 11)
940	3	37.6 + 14.8	650	4	(37.6 + 37.6) + (14.8 + 14.8)
1160	2	56 + 22.1	900	3	(56 + 56) + (22.1 + 22.1)

was carried out with a normal load of 2.5 N. In order to study the influence of time on the wear behaviour, the tests were performed at room temperature, in air and for different times: 2, 5, 10 and 15 min.

A scratch tester equipment (CSEM Revetest) was used to get information on the adhesion of the coating to the substrate. The test consists of introducing stress by deforming the surface by means of indentation with a Rockwell C diamond tip (angle of 120° and a radius of 0.2 mm). The applied load is increased continuously until film detachment (maximum load = 60 N). The critical load L_C is defined as the smallest load at which the coating is damaged. The scratches were made at a loading rate of 100 N mm^{-1} and a diamond tip velocity of 10 mm min^{-1}.

Topographic readings of wear tracks were measured with a monitored three-dimensional tactile profilometer composed of a diamond stylus with a conic shape (radius of 1.25 μm). The sample was moved with a computer-controlled horizontal scanning system, providing an examination following the x and y perpendicular directions.

2.3. *Structural measurements*

Scanning electron microscopy (SEM), with a JEOL 5800LV instrument, was used to study the interface morphology and cross-sections of the multilayered coatings. Surface topography was analysed by atomic force microscopy (AFM) with a Topometrix explorer in non-contact mode. Root-mean-square (RMS) roughness of the surface was also determined (with flatting corrections).

The depth profiles of titanium, aluminium and nitrogen elements in the multilayers (type I and type II) were performed by glow discharge optical emission spectroscopy (GDOES) using a GDS 750 spectrometer (LECO). The argon glow discharge was supplied by a voltage of $U_{DC} = 700$ V (regulation of the argon flow rate to set $I = 20$ mA) and with an anode diameter of 4 mm. The emission lines of Fe^{I} at 371.994 nm for the substrate, and N^{I} at 174.272 nm, Ti^{I} at 337.279 nm and Al^{I} at 396.152 nm for the films, have been measured.

3. Results

3.1. *GDOES depth profiling*

The GDOES emission line intensities of each species as a function of the erosion time for TiN/AlN multilayer type I with $\Lambda = 360$ nm and for sample type II with $\Lambda = 240$ nm are shown in Fig. 1(a) and (b), respectively. Profile evolution reveals alternating of titanium- and aluminium-rich layers where the titanium maximum intensity coincides with an aluminium minimum inten-

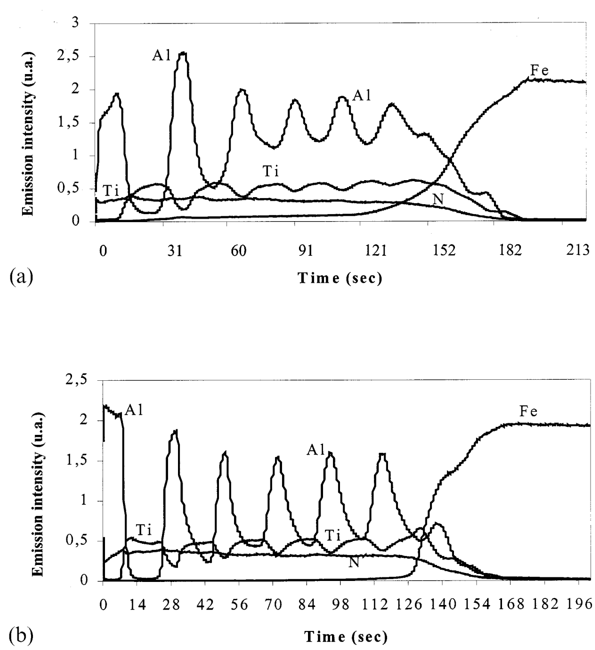

Fig. 1. DC GDOES depth profile of TiN/AlN multilayers. Some differences of regularity and sharpness of interfaces between multilayers of type I (a) and type II (b) can be noticed. The periodicity is (a) $\Lambda = 360$ nm and (b) $\Lambda = 240$ nm.

sity. The number of single layers and bilayers can easily be counted. It is worth mentioning that the regularity of the periods appears to decrease with the erosion depth. This phenomenon can be explained by an anisotropic sputtering effect during the formation of the crater. In fact, irregular erosion rates such as trenching (a deep groove eroded around the edge of the crater) or bowling (a hollowing of the centre of the crater to produce a concave surface) are sometimes observed with this analytical method [27–30]. These effects can lead to incorrect values for the atomic elemental distribution. This effect is particularly serious for multilayers with a short periodical structure.

Nevertheless, coatings of type II [Fig. 1(b)] exhibit a more regular profile than coatings of type I. Assuming that the erosion craters referred to previously have the

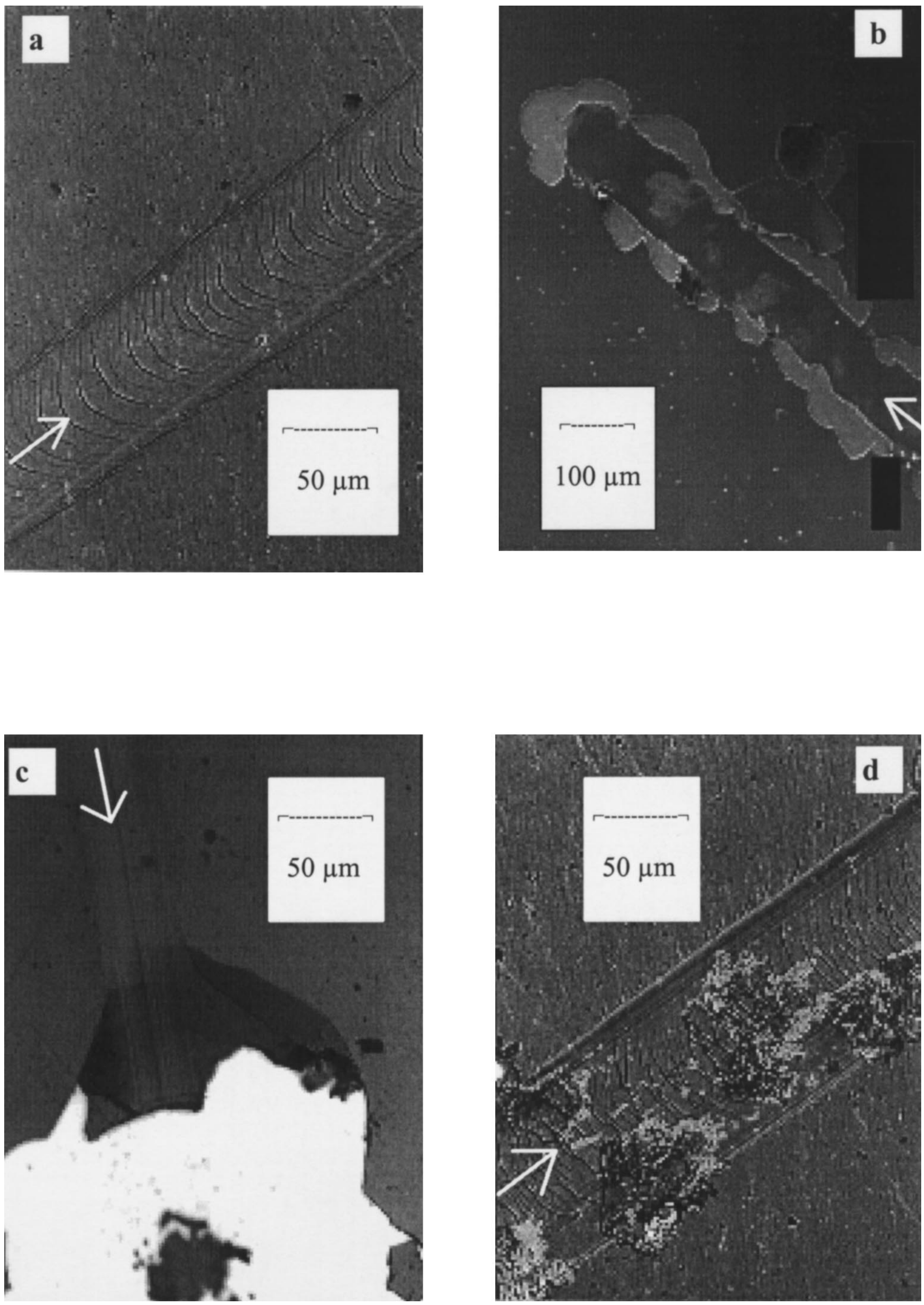

Fig. 2. Optical (a, b, c) and SEM (d) observations of the wear tracks obtained by scratch tests for type II (a, b, d) and type I (c) films. Elastic and plastic deformations of the multilayered material can readily be distinguished. Arrows indicate the sliding direction of the stylus.

same size, the sharper profile distribution measured for coatings of type II is typical of the deposition mode.

3.2. Adhesion

The scratch test implies elastic and plastic deformation until the coating and the substrate are separated. In general, processes of cohesive (cracking) and adhesive (flaking) failures of multilayered coatings are observed [31–34].

A different behaviour between the wear tracks of types I and II TiN/AlN multilayers is noticed in Fig. 2. Indeed, for samples of type I, the critical load does not exceed $L_C = 18$ N (Fig. 3) and flaking of the coating takes place immediately after the beginning of the scratch test [Fig. 2(c)]. In addition, for samples of type II, several mechanisms responsible for the failure and delamination can be identified [Fig. 2(d)]. At first, the elastic deformation of the coating–substrate system due to the sliding diamond tip does not produce any visible surface damage. With an increasing normal loading force, cracks appear. Two types of crack are observed: external parallel cracks that occur along the sides of the scratch and internal transverse cracks with a semicircular geometry [Fig. 2(a)]. Finally, for higher normal loading forces, a discontinuous chip removal happens.

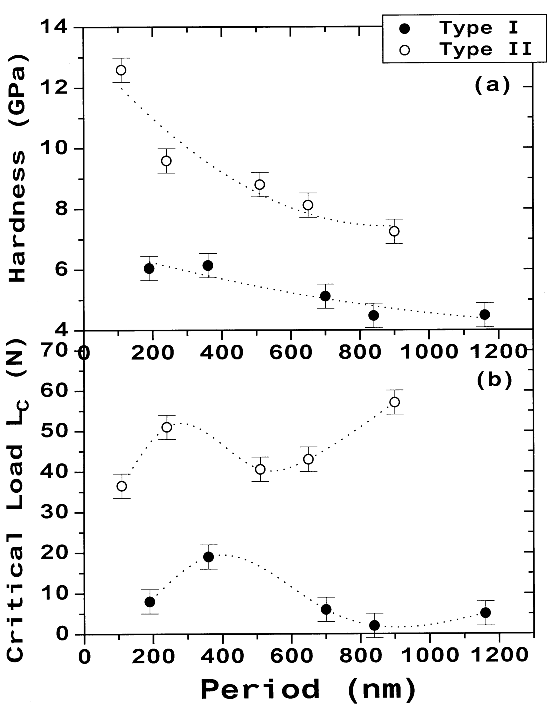

Fig. 3. (a) Hardness as a function of the period thickness Λ of TiN/AlN films. Hardness can be improved at first when the period is reduced but the most significant effect is obtained when an ion bombardment is applied between the deposition of each layer. (b) Critical load L_C of TiN/AlN films measured from the scratch test. For the two sample series, the period thickness Λ does not really influence L_C. On the other hand, this latter is increased strongly for samples of type II.

For all multilayered coatings, two mechanisms of damage by flaking appear. The adhesive lateral flaking observed systematically for the type II multilayers seems to reveal a weak rate of compressive stresses. Moreover, the semicircular flakes observed in front of the tip in Fig. 2(b) (noticed for the type I multilayers) correspond to an excessive accumulation of compressive stresses and lead to detachment of the whole coating.

3.3. Hardness and Young's modulus

For both types of sample, the hardness decreases with increasing period thickness Λ (Fig. 3), in agreement with the general trend found in the literature ($\text{hardness}_{\text{TiN}} = 12$ GPa and $\text{hardness}_{\text{AlN}} = 6.3$ GPa) [23,26,35–43].

It is important to notice that samples of type II exhibit a higher hardness than type I samples for every period. This mechanical improvement is especially enhanced when the period thickness decreases; it reaches 12.5 GPa for $\Lambda = 120$ nm. The beneficial role of the ion bombardment is clearly proved from these results.

From the hardness measurements, the Young's modulus E is deduced by assuming a constant Poisson's ratio $\nu = 0.3$ for the overall multilayers. The influence of the bombardment and period thickness are shown in Fig. 4. Since Young's modulus is directly correlated to macroscopic mechanical properties, it can be said that samples of type II appear less elastic and harder than those of type I. Moreover, the absence of radial cracks on the indentation imprint confirms the plastic character of type II multilayers.

3.4. Wear resistance

No variation of the coefficient of friction μ (ratio of the friction force divided by the normal force [31]) of

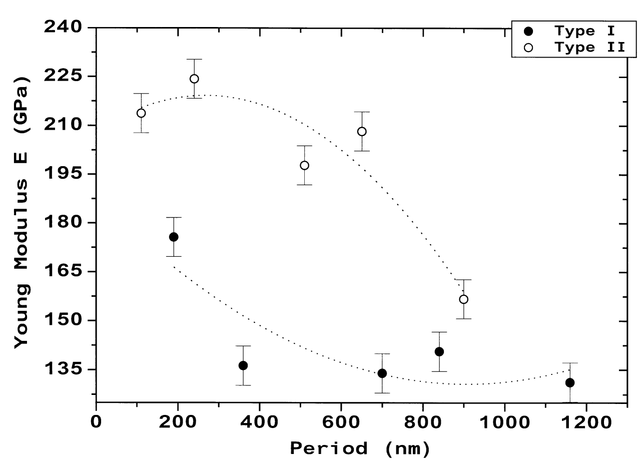

Fig. 4. Influence of period Λ on the overall Young's modulus E for both types of sample. The bombardment of each layer leads to higher plastic behaviour of the coatings.

TiN/AlN coatings as a function of the period thickness Λ has been observed in this study. It remains constant near 0.6 for I and II multilayers. Nevertheless, the track width obtained with the tribometer increases with the period. In fact, the thicker the AlN layer (soft material), the deeper the friction ball enters into the coating. Moreover, the longer the rub on the surface, the higher the interfacial stresses. To estimate the stress rate, we first assumed that its magnitude corresponds to the occurrence of sample flaking. Two typical three-dimensional profiles obtained with type I and II films are presented in Fig. 5. From these measurements and taking into account the length and wear volume of the track, the wear rate K can be obtained with the following relationship:

$$K=\frac{V_{\text{wear}}}{F\times L}, \tag{1}$$

where K=wear rate ($\text{mm}^3\,\text{N}^{-1}\,\text{m}^{-1}$), V_{wear}=wear volume (mm^3), F=normal force applied (N) and L= total sliding length (m).

Wear rates have been calculated for both sample series prepared with various total periods Λ, and the effect of the wear time has been investigated also (Table 3). For both types of sample, the whole coating is immediately removed (delamination) after the first passage of the ball and this phenomenon occurs for every period Λ. Due to a low wear resistance, the substrate is directly in contact with the ball.

For type II multilayers, the wear rate increases with the wear time and, for the shortest thickness period ($\Lambda=120$ nm), K remains below $0.1\times10^{-3}\,\text{mm}^3\,\text{N}^{-1}\,\text{m}^{-1}$ until the wear time reaches 10 min. Above

Table 3
Variation of wear rates $10^{-3}\times$ K ($\text{mm}^3\,\text{N}^{-1}\,\text{m}^{-1}$) of type II multilayers as a function of the period thickness Λ for various wear times

Wear time (min)	Period, Λ ($\pm$10 nm)				
	110	240	510	650	900
2	0.10	0.13	0.17	0.17	0.26
5	0.10	1.28	1.66	1.74	2.60
10	0.12	1.33	3.94	2.69	3.91
15	1.92	1.40	5.33	2.53	4.18

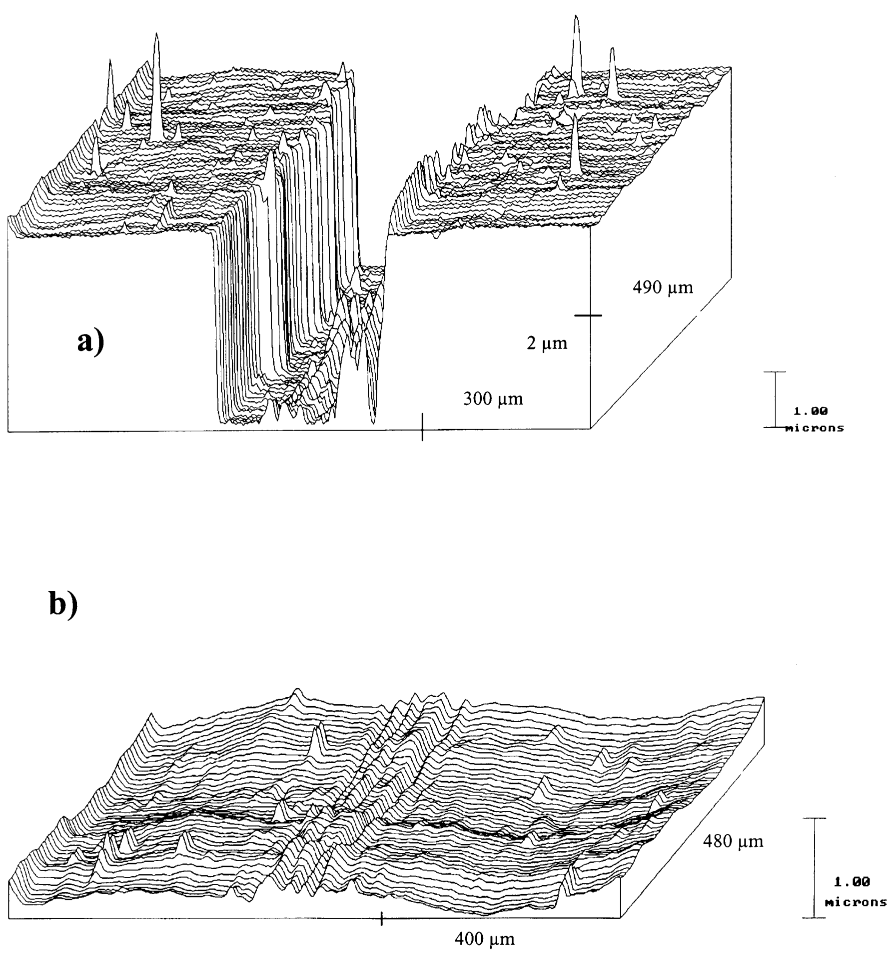

Fig. 5. Topographic analyses of wear tracks obtained on TiN/AlN multilayers. The same test parameters have been used for type I (a) and type II (b) samples with a period thickness $\Lambda=120$ and 190 nm, respectively.

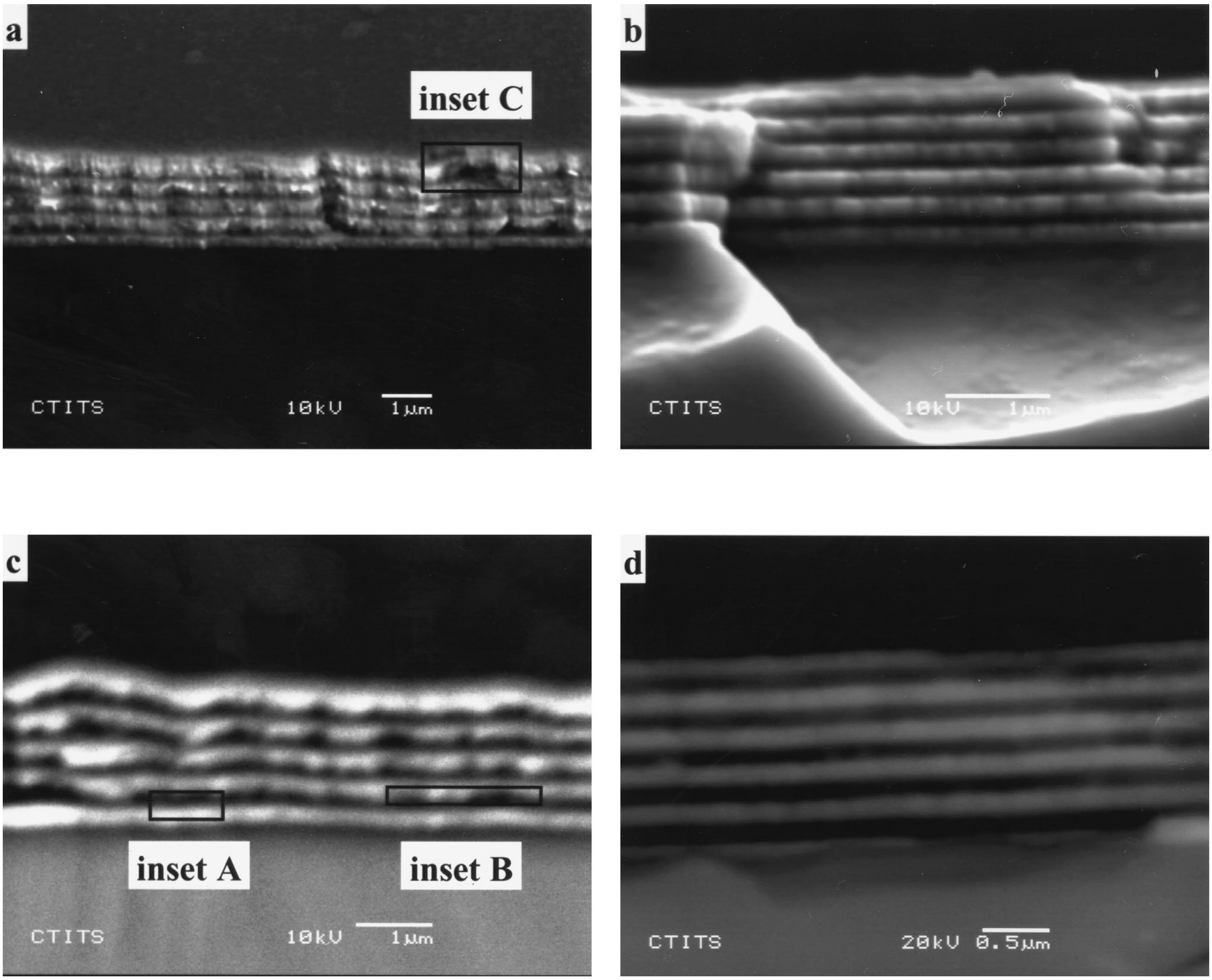

Fig. 6. SEM photographs of TiN/AlN multilayers on cross-sectional views. Microstructure and interfaces are compared between type I (a, c) and type II (b, d). The period thickness is $\Lambda=510$ and 420 nm for (a, c) and (b, d), respectively. Improvement of interface quality is easily distinguished (TiN layers are bright whereas AlN are dark).

this time and for each period Λ, layers are completely debonded and delaminated.

In previous works, it has been shown when a steel ball was in sliding contact against a ceramic coating (TiN and TiCN, 3 μm thick) [44–46], an important transfer of material from the ball to the ceramic occurred. This phenomenon indicates that the ball suffers adhesive wear. In addition, a large amount of oxygen was detected showing that oxidation occurs during friction. In the present study we did not detect any transfer from the ball on the ceramic surface. Only oxygen was detected on the rubbing surfaces. The absence of metal transfer on the coated sample is probably due the fact that when the steel ball slides on the surface, shear stress may act at the TiN/AlN interface leading to removal of the AlN top layer. The energy of adhesion between the different layers is lower than the cohesive energy of each of the two materials (TiN, AlN) and that of 100C6 steel. This may explain why the steel ball did not suffer adhesive wear as was mentioned in the case of TiN or TiCN coatings.

3.5. Interface investigations

Multilayer interfaces depend strongly on the nucleation and growth mechanisms of each layer on the other. In order to investigate the effects of layer thickness and ion bombardment on the morphology and interfaces of the films, cross-sectional SEM and AFM topographic measurements were analysed.

In Fig. 6(a) and (b), typical views of TiN/AlN multilayers deposited on a (100) silicon wafer can be seen for type I and type II samples, respectively. Because of the different electronic emission coefficients for titanium and aluminium (atomic number differences), TiN (bright) and AlN (dark) layers are easily identified by using the electronic secondary detection of SEM. The thickness of each TiN and AlN layer or the total coating thickness is not accurately measurable from these photographs because of the tilted observation of the coatings. In addition, the sample breaking carried out just before introducing it in the SEM chamber rarely leads to a clean and perpendicular fracture. Nevertheless, interesting features of the microstructure are observed in each layer. For type I multilayers, TiN layers exhibit a more columnar-like morphology than AlN. From structure zone models [47,48] it is expected that, for a substrate at room temperature, sputter-deposited TiN coatings tend to adopt a stronger columnar structure than AlN since the melting point of TiN is higher than that of AlN ($mp_{TiN}=2930$ K and $mp_{AlN}=2200$ K).

From the SEM observations of samples of type I, it is also interesting to notice that TiN/AlN and AlN/TiN interfaces present some contrasts. As an example, the AlN/TiN interfaces in Fig. 6(c) appear less rough than the reverse interfaces. The dark–bright edges as shown in inset B are not so clear and sharp as the opposite edges seen in inset A. According to SEM investigations, the contact surface between each layer is different. This influences the adhesion properties of one layer on the other. One can suggest that a TiN coating deposited on an AlN surface leads to worse interface quality than the reverse deposition. Inset C in Fig. 6(a) shows an example of separation of a TiN layer. This detachment of TiN from AlN was observed for every multilayer of type I and for any period thickness Λ.

Fig. 6(b) and (d) clearly show the effect of ion bombardment on the quality of the interface roughness. The TiN layer is easily identified (bright layer), as well as the number of layers. Irregularities and defects previously noticed at TiN/AlN interfaces for samples of type I are not visible. The shapes and features of TiN as well as AlN layers appear clearly. The interface roughness is lowered.

In order to evidence the influence of ion bombardment on the interface morphologies of layers, the surface topography of TiN and AlN single layers has been analysed by AFM. Typical plane views of 200 nm thick TiN and AlN coatings deposited on (100) silicon wafers with and without a post layer-deposition ion bombardment are shown in Fig. 7. A non-bombarded TiN surface [Fig. 7(a)] shows near-spherical nodules (30–50 nm) mostly disconnected from each other and lightly coalescent. A non-bombarded AlN surface [Fig. 7(c)] exhibits smaller and less bumpy particles with a more compact macroscopic structure. A smaller RMS roughness is also measured for aluminium nitride: 1.5 nm against 5.2 nm for titanium nitride.

In the case of bombarded surfaces [Fig. 7(b) and (d)], the surface topography is largely eroded and flattened since RMS roughness is reduced to 1.9 nm and 0.9 nm for TiN and AlN, respectively. Resputtering of the layers occurs, which is much more significant for AlN coatings.

4. Discussion

GDOES profile measurements clearly show the periodic microstructure of layers containing titanium and aluminum. Since the nitrogen partial pressure during the deposition is large enough to completely poison the titanium and aluminium targets [49–55], it is expected to obtain nearly stoichiometric TiN and AlN compounds [50,51]. For both spectra presented in Fig. 1, the nitrogen signal is nearly constant through the whole thickness. Since GDOES gives qualitative information only, no significant value can be deduced for the composition. Modelling of TiN and AlN erosion rates is required to get a quantitative depth profile analysis of each element [27]. However, the shape of GDOES intensity peaks observed for the aluminium and titanium signals in the case of films of type I indicate that the morphology of the TiN layer is less homogeneous than that of the AlN layer. For films of type II, titanium and aluminium profiles display peaks with slightly unsymmetrical shapes on the right peak side. This suggests a sharp TiN/AlN interface whereas the reverse interface AlN/TiN is more intermixed. In addition, the ion bombardment is expected to induce preferential nitrogen resputtering. This generates point defects (nitrogen vacancies) on the surface and a metal enrichment. Since the strength of the Al—N chemical bond (297 kJ mol^{-1}) is weaker than that of TiN (476 kJ mol^{-1}), one can understand the abruptness of the aluminium line emission on the left peak side.

The present results support the importance of the interface structure for the properties of multilayered coatings. Other investigations show that, during an ion-assisted deposition, various effects take place leading to some structural and morphological modifications of the layers. Four kinds of phenomena are usually identified: surface desorption, densification, resputtering and implantation [56–59]. The predominant influence depends primarily on the ion energy and ion-current density [60,61]. In our case, the experimental conditions are different because the ion bombardment is not applied during deposition. However, argon-ion energy and current density are also fundamental parameters for a simple etching operation. In this study, the ion bombardment does not lead solely to erosion and a smoothing effect of the surface as clearly observed by AFM; it also modifies physical and chemical properties of the surface layer. With the flattening of each layer, the nucleation density of the next material to be deposited increases [62,63], and the number of voids and the void volume fraction at the interfaces are decreased. Hence, contacts and sticking between each nitride are improved.

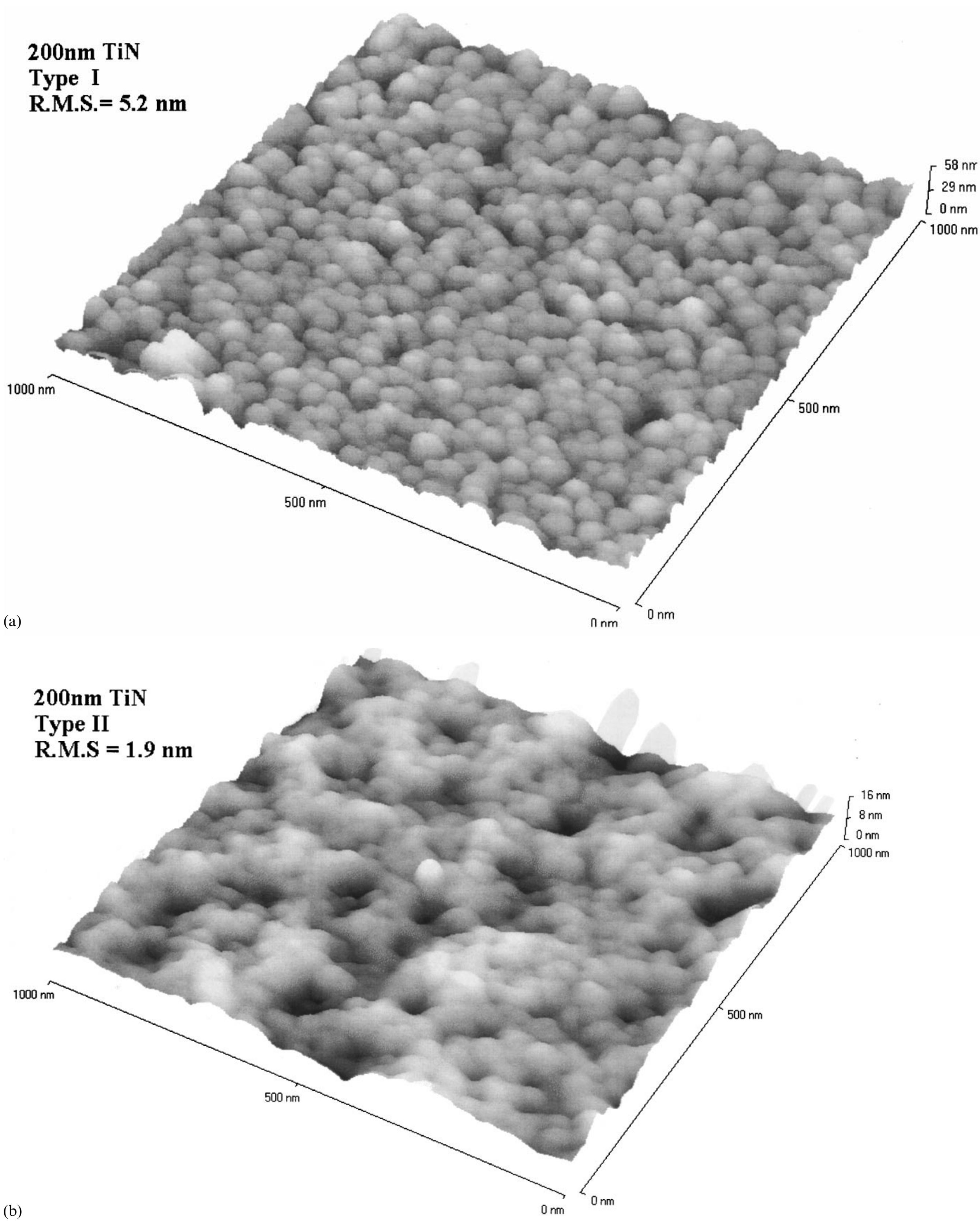

Fig. 7. Surface morphology of TiN and AlN single layers (200 nm thick) observed by AFM. Ion bombardment of titanium nitride (b) and aluminium nitride (d) induces erosion and smoothening of the surface. Roughness is reduced and topography evolution can be compared with that of non-bombarded TiN (a) and AlN (c). The vertical axis is different in all partial figures.

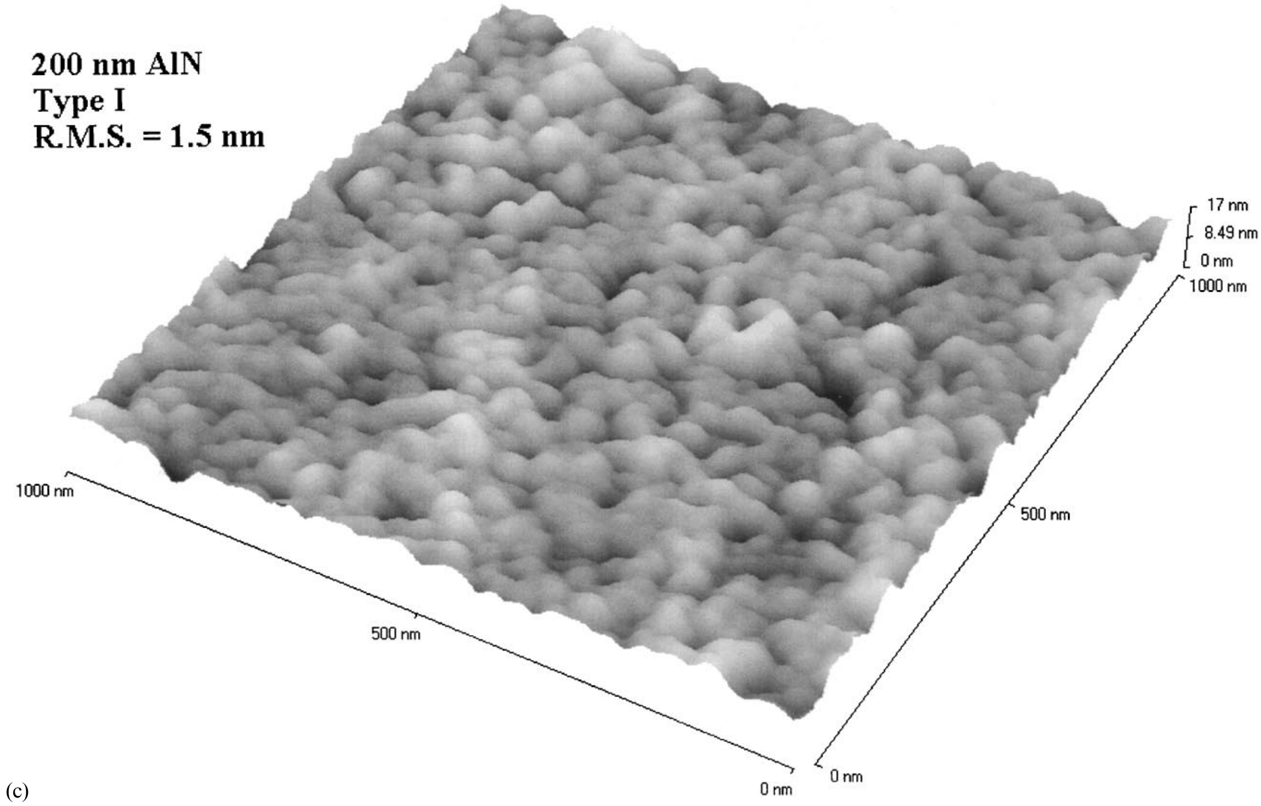

(c)

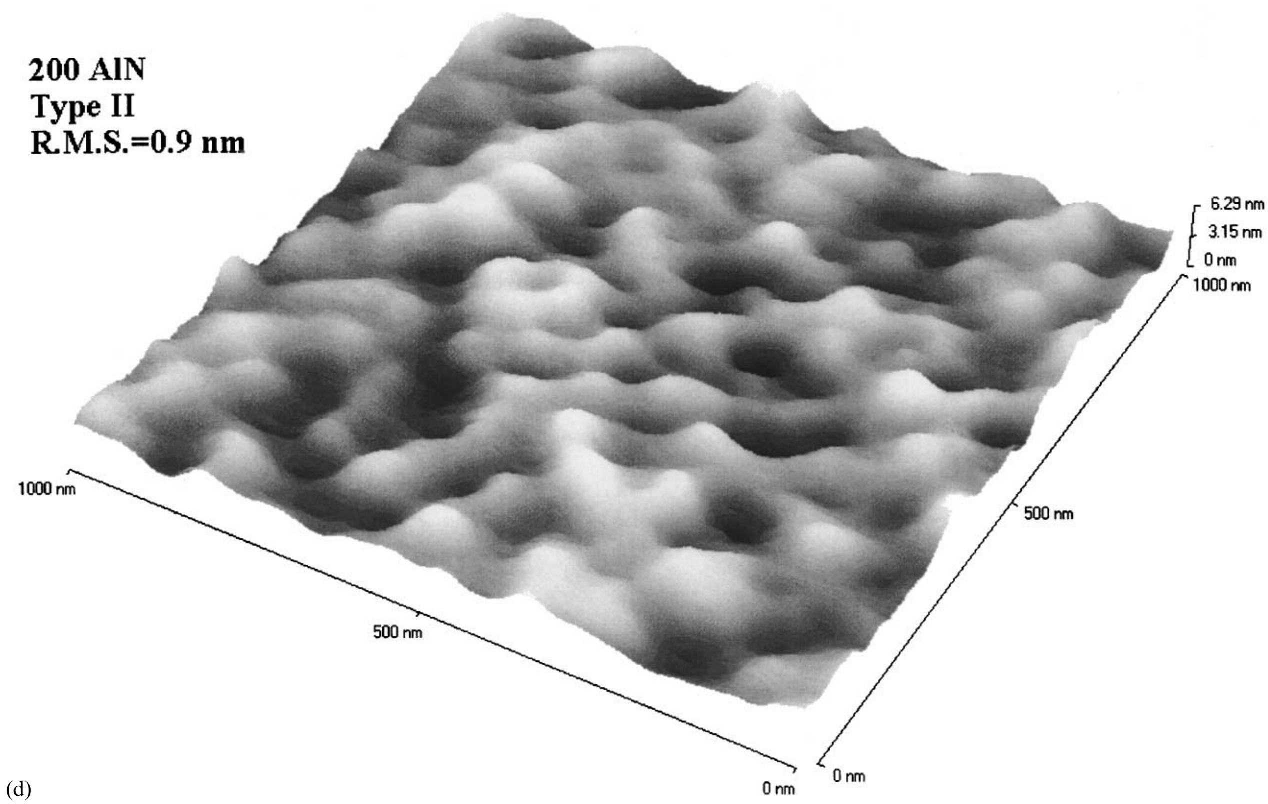

(d)

Fig. 7. (*continued*)

Moreover, ion bombardment can also lead to a modification of the nitrogen content in each sub-layer. In order to evidence the influence of ion bombardment on the stoichiometry of layers, TiN/AlN multilayer systems and TiN and AlN single layers have been analysed by Rutherford backscattering spectrometry (RBS). RBS analyses of TiN and AlN single layers clearly show no modification of the stoichiometry (close to $TiN_{1.0}$ and $AlN_{1.0}$). For TiN/AlN multilayers the evolution of the experimental RBS spectra for different numbers of bilayers is very difficult to reproduce with simulations. In fact, RBS itself is revealed to be sensitive to the stoichiometry and thickness of each layer, to the interfacial roughness between sub-layers and to the average interlayer roughness (broadening of the intermixing zone). The complexity of various mechanisms and phenomena occurring at the interfaces increases the difficulty in determining the profile composition of multilayers and in better understanding the structure of the TiN/AlN multilayer.

From the investigations of Clemens et al. [36], the hardness of multilayers can be examined according to the total period thickness $\Lambda=\lambda_{\mathrm{TiN}}+\lambda_{\mathrm{AlN}}$. Typically, variation of the hardness versus $1/\Lambda^{1/2}$ is plotted and fits can be performed to the linear region. Hardness evolution against $1/\Lambda^{1/2}$ is illustrated in Fig. 8 for both types of sample. A linear variation is obtained in agreement with the following relationship:

$$H=H_0+\frac{k_{\mathrm{HP}}}{\sqrt{\Lambda}}, \tag{2}$$

where H_0 and k_{HP} are experimental constants.

At first, H_0 is representative of the hardness of the single-component constituent films. The high H_0 values also reflect the resistance to dislocation motion in the individual layers of the multilayer independent of the effect of layering [36]. For samples of type I and II, H_0 values are quite similar (5.5 and 3.8, respectively). The slope k_{HP} is representative of the difficulty in forcing dislocations through the interface between the layers [36]. Linear fits in Fig. 8 show that the slope is higher for samples of type II. The ion bombardment improves the quality of interfaces, and so the motion of dislocations between sub-layers becomes increasingly difficult.

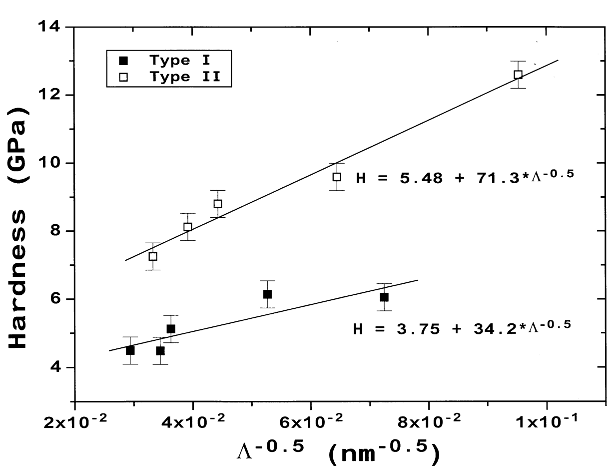

Fig. 8. Plot of hardness as a function of $1/\Lambda^{1/2}$ for types I and II TiN/AlN multilayers. The difference between the slope values is closely linked to the beneficial role of ion bombardment.

5. Conclusion

TiN/AlN multilayered coatings have been reactively deposited by DC magnetron sputtering with and without ion bombardment between the deposition of each successive layer. The mechanical properties of these multilayered coatings depend strongly on the period thickness. If it is true that the final features of the overall periodical system are first of all linked to the nature of each single layer, they are also influenced by a suitable and an efficient association of the compounds (synergistic effect of both material behaviours). In order to ensure this beneficial association, interfaces must be taken into account as much as single-layer properties.

A great improvement of the physical and tribological properties of TiN/AlN multilayers was obtained when an intermediary ion bombardment of every sub-layer surface was applied between each deposition. This beneficial treatment is attributed mainly to an enhancement of interfacial quality and roughness.

Many studies about the synthesis of multilayers with well-controlled structure have shown that their interesting and promising performances are the result of a combination of effects like growth mechanisms, microstructure differences of the components or stresses. The present study supports the crucial importance of interfaces.

Acknowledgements

The authors thank DUPM (District Urbain du Pays de Montbéliard) for financial support and CTITS (Centre de Tranfert Industriel en Traitements de Surface) for technical assistance. They are also grateful to F. Thelisson and H. Souissi from the research centre of PSA Belchamps for mechanical and tribological measurements.

References

[1] H.A. Jehn, B. Rother, Int. J. Refract. Met. Hard Mater. 14 (1996) 87.
[2] H.A. Jehn, S. Hofmann, W.D. Münz, Thin Solid Films 153 (1987) 45.

[3] E. Vancoille, J.P. Celis, J.R. Roos, Thin Solid Films 224 (1993) 168.
[4] S. Jiang, D. Peng, X. Zhao, L. Xie, Q. Li, Appl. Surf. Sci. 84 (1995) 373.
[5] S. Inoue, H. Uchida, A. Hioki, K. Koterazawa, R.P. Howson, Thin Solid Films 271 (1995) 15.
[6] O. Knotek, W.D. Münz, T. Leyendecker, J. Vac. Sci. Technol. A 5 (1987) 2173.
[7] T. Leyendecker, O. Lemmer, S. Esser, J. Ebberink, Surf. Coat. Technol. 48 (1991) 175.
[8] R. Wuhrer, W.Y. Yeung, M.R. Phillips, G. McCredie, Thin Solid Films 290–291 (1996) 339.
[9] L. Cunha, M. Andritschky, L. Rebouta, R. Silva, Thin Solid Films 317 (1998) 351.
[10] H. Jensen, J. Sobota, G. Sorensen, J. Vac. Sci. Technol. A 15 (1997) 941.
[11] J.H. Hsieh, C. Liang, C.H. Yu, W. Wu, Surf. Coat. Technol. 108–109 (1998) 132.
[12] C.J. Tavares, L. Rebouta, B. Almeida, J. Bessa e Sousa, Surf. Coat. Technol. 100–101 (1998) 65.
[13] H. Jensen, J. Sobota, G. Sorensen, J. Vac. Sci. Technol. A 16 (1998) 1880.
[14] C.J. Tavares, L. Rebouta, B. Almeida, J. Bessa e Sousa, M.F. da Silva, J.C. Soares, Thin Solid Films 317 (1998) 124.
[15] O. Knotek, F. Löffler, G. Krämer, Surf. Coat. Technol. 59 (1993) 14.
[16] W.D. Sproul, J. Vac. Sci. Technol. A 12 (1994) 1595.
[17] X. Zeng, S. Zhang, J. Hsieh, Surf. Coat. Technol. 102 (1998) 108.
[18] N. Martin, C. Rousselot, Surf. Coat. Technol. 110 (1998) 158.
[19] J.A. Thornton, J.E. Greene, in: R.F. Bunshah (Ed.), Handbook of Deposition Technologies for Films and Coatings, Noyes Publications, Park Ridge, NJ, 1994, p. 29.
[20] I. Wadsworth, D.B. Lewis, G. Williams, J. Mater. Sci. 31 (1996) 5907.
[21] M. Nordin, M. Larsson, S. Hogmark, Surf. Coat. Technol. 106 (1998) 234.
[22] Z. Czigany, I. Kovacs, G. Radnoczi, Thin Solid Films 317 (1998) 266.
[23] L.A. Donohue, J. Cawley, D.B. Lewis, J.S. Brooks, W.D. Münz, Surf. Coat. Technol. 76–77 (1995) 149.
[24] Y. Haga, O. Nittono, Thin Solid Films 281–282 (1996) 132.
[25] T. Hurkmans, T. Trinh, D.B. Lewis, J.S. Brooks, W.D. Münz, Surf. Coat. Technol. 76–77 (1995) 159.
[26] M. Shinn, L. Hultman, S.A. Barnett, J. Mater. Res. 7 (1992) 901.
[27] Z. Weiss, J. Anal. Atom Spectrom. 10 (1995) 891.
[28] Z. Weiss, K. Marshall, Thin Solid Films 308–309 (1995) 382.
[29] M. Ives, D.B. Lewis, C. Lehmberg, Surf. Interface Anal. 25 (1997) 191.
[30] U. Beck, G. Reiners, Th. Wirth, V. Hoffmann, F. Präßler, Thin Solid Films 290–291 (1996) 57.
[31] F. Attar, T. Johannesson, Surf. Coat. Technol. 78 (1996) 87.
[32] M. Larsson, M. Bromark, P. Hedenqvist, S. Hogmark, Surf. Coat. Technol. 76–77 (1995) 202.
[33] K.J. Ma, A. Bloyce, T. Bell, Surf. Coat. Technol. 76–77 (1995) 297.
[34] P. Hedenqvist, M. Olsson, S. Jacobson, Surf. Coat. Technol. 41 (1990) 31.
[35] R.C. Cammarata, T.E. Schlesinger, C. Kim, S.B. Qadri, A.S. Edestein, Appl. Phys. Lett. 56 (1990) 1862.
[36] B.M. Clemens, H. Kung, S.A. Barnett, MRS Bull. 24 (2) (1999) 20.
[37] U. Helmersson, S. Todorova, S.A. Barnett, J.E. Sundgren, L.C. Market, J.E. Greene, J. Appl. Phys. 62 (1987) 481.
[38] E. Kusano, M. Kitagawa, H. Nanto, A. Kinbara, J. Appl. Phys. A 16 (1998) 1272.
[39] I. Manika, F. Muktepavela, H. Jensen, J. Sobota, G. Sorensen, Surf. Coat. Technol. 100–101 (1998) 333.
[40] P.B. Mirkarimi, L. Hultman, S.A. Barnett, Appl. Phys. Lett. 57 (1990) 2654.
[41] K.K. Shih, D.B. Dove, Appl. Phys. Lett. 61 (1992) 654.
[42] J.E. Sundgren, J. Birch, G. Hakansson, L. Hultman, U. Helmersson, Thin Solid Films 193–194 (1990) 819.
[43] P. Yashar, S.A. Barnett, J. Rechner, W.D. Sproul, J. Vac. Sci. Technol. A 16 (1998) 2913.
[44] J. Takadoum, H. Houmid Bennami, Surf. Coat. Technol. 96 (1997) 272.
[45] I.L. Singer, S. Fayelle, P.D. Ehni, Wear 149 (1999) 375.
[46] J. Takadoum, H. Houmid Bennami, M. Allouard, Surf. Coat. Technol. 88 (1996) 232.
[47] B.A. Movchan, A.V. Demchishin, Fiz. Metal. Metalloved 28 (1969) 653.
[48] J.A. Thornton, J. Vac. Sci. Technol. 11 (1974) 666.
[49] S. Berg, H.O. Blom, T. Larsson, C. Nender, J. Vac. Sci. Technol. 15 (1987) 202.
[50] S. Berg, T. Larsson, C. Nender, H.O. Blom, J. Vac. Sci. Technol. A 6 (1988) 1832.
[51] S. Berg, T. Larsson, C. Nender, H.O. Blom, J. Appl. Phys. 63 (1988) 887.
[52] H. Ofner, R. Zarwaasch, E. Rille, H.K. Pulker, J. Vac. Sci. Technol. A 9 (1991) 2795.
[53] E.J. Bienk, H. Jensen, G.N. Pedersen, G. Sorensen, Thin Solid Films 230 (1993) 121.
[54] S. Hofman, Thin Solid Films 191 (1990) 335.
[55] J. Musil, S. Kadlec, J. Vyskocil, V. Poulek, Surf. Coat. Technol. 39–40 (1989) 301.
[56] N. Martin, D. Baretti, C. Rousselot, J.Y. Rauch, Surf. Coat. Technol. 107 (1998) 172.
[57] F.A. Smidt, Int. Mater. Rev. 35 (1990) 61.
[58] N. Marechal, E. Quesnel, Y. Pauleau, J. Electrochem. Soc. 141 (1994) 1691.
[59] J.M.E. Harper, J.J. Cuomo, R.J. Gambino, H.R. Kaufman, in: O. Auciello, R. Kelly (Eds.), Ion Bombardment Modification of Surfaces, Elsevier, Amsterdam, 1984, p. 127.
[60] J.L. Vossen, J.J. Cuomo, in: J.L. Vossen, W. Kern (Eds.), Thin Film Processes, Academic Press, New York, 1978, p. 207.
[61] R.A. Roy, A. Yee, in: J.J. Cuomo, S.M. Rossnagel, H.R. Kaufman (Eds.), Handbook of Ion Beam Technology, Noyes Publications, Park Ridge, NJ, 1989, p. 194.
[62] J.E. Greene, in: T.S. Moss, S.P. Keller (Eds.), Handbook of Semiconductors, North Holland Publishing Company, Amsterdam, 1980, p. 499.
[63] K. Reichelt, Vacuum 38 (1988) 1083.